Coherence loss and revivals in atomic interferometry: a quantum-recoil analysis



2012 J. Phys. A: Math. Theor. 45 165303

(http://iopscience.iop.org/1751-8121/45/16/165303)

J. Phys. A: Math. Theor. **45** (2012) 165303 (17pp) doi:10.1088/1751-8113/45/16/165303

# Coherence loss and revivals in atomic interferometry: a quantum-recoil analysis

**M Davidović[1], A S Sanz[2], M Božić[3] and D Arsenović[3]**

[1] Faculty of Civil Engineering, University of Belgrade, Bulevar Kralja Aleksandra 73, 11000 Belgrade, Serbia
[2] Instituto de Física Fundamental (IFF—CSIC), Serrano 123, 28006 Madrid, Spain
[3] Institute of Physics, University of Belgrade, Pregrevica 118, 11080 Belgrade, Serbia

E-mail: asanz@iff.csic.es

Received 4 January 2012, in final form 4 March 2012
Published 4 April 2012
Online at stacks.iop.org/JPhysA/45/165303

**Abstract**
The coherence effects induced by external photons coupled to matter waves inside a Mach–Zehnder three-grating interferometer are analyzed. Alternatively to atom–photon entanglement scenarios, the model considered here only relies on the atomic wavefunction and the momentum shift induced in it by the photon scattering events. A functional dependence is thus found between the observables, namely the fringe visibility and the phase shift, and the transversal momentum transfer distribution. Good quantitative agreement is found when comparing the results obtained from our model with the experimental data.

PACS numbers: 03.65.Ta, 03.75.Dg, 42.50.−p, 42.50.Xa, 37.25.+k, 42.25.Hz

(Some figures may appear in colour only in the online journal)

## 1. Introduction

The remarkable refinement reached in matter wave interferometry in recent decades [1, 2] has made it possible to explore experimentally fundamental key questions about wave particle duality and complementarity that have been studied since the very inception of quantum mechanics [3, 4]. In this regard, Chapman *et al* [5] carried out an outstanding experiment in 1995, where the influence of photon–atom scattering events (inside an atomic Mach–Zehnder interferometer) on the coherence properties of an atomic beam was investigated. This experiment was interpreted as a realization with atoms of Feynman's 'which-way' *gedankenexperiment* [6].

The most intriguing result from Chapman's experiment was the revival of fringe contrast beyond the limits predicted by the complementary principle [2, 5, 7]. Furthermore, a regain of fringe contrast after post-selecting atoms at the exit of the interferometer according to the momentum transferred in the photon–atom scattering process was also observed [5]. The

  

regain of interference due to post-selection in momentum space had been previously reported for optical [8] and neutron [9] experiments with the presence of resonant spin-flipper fields. In the case of the neutron experiments, a spectral modulation effect was observed by means of a proper post-selection procedure, where the spatial shift of the wave trains greatly exceeds the coherence length of the neutron beams traversing the interferometer [1, 9].

By the time the paper by Chapman *et al* [5] was published, a controversy on the origin of the disappearance of interference in 'which-way' (actually, 'which-slit') double-slit experiments was already in fashion: recoil versus decoherence. At a first glance, it seems that the primacy of recoil arguments [10] has been contested in favor of more general decoherence mechanisms, based on considering the entanglement between the observed system and its environment to be the source of the system loss of fringe contrast or visibility. Nevertheless, Storey *et al* [11] argued that, whenever interference is destroyed, transverse momentum has to be transferred according to the uncertainty principle.

Revivals observed beyond the limit of the complementarity principle enforced Chapman *et al* [5] and Cronin *et al* [2] to argue that 'the momentum recoil by itself cannot explain the loss of contrast (as it can in the diffraction experiments), but the path separation at the point of scattering and the phase shift imprinted by the entanglement in the scattering process must also be taken into account'. In addition, Cronin *et al* [2] argued that 'focusing on the which-way information carried away by the scattered photons is not the only way decoherence may be understood. An alternative, but completely equivalent picture involves the phase shift between the two components of the atomic wavefunction'. These two views (which-way and dephasing) 'correspond to two different ways to describe the scattered photon (position basis versus momentum basis). In these two cases, an observer in the environment can determine either which path the atom took or else the phase shift of its fringe pattern. The key point is that when the experimenter is completely ignorant of the state of the scattered photons, whether an apparatus has been set up to measure them or not, the which-path and phase diffusion pictures are equally valid (Stern *et al* 1990, [12]). Both predict decoherence, i.e. the loss of contrast' [2].

It is important to note that the apparatus of Chapman *et al* [5] was set up to detect atoms, but not to measure the state of the scattered photons. Because of this, in this work we study this experiment using a model [13, 14] that focuses on atomic states. It accounts for the effects caused on the atom time-dependent wavefunction by the interferometer as well as the (environmental) photons scattered from the atoms when the latter are excited in a resonance fluorescence state by a laser beam. Due to the negligible timescales involved in the dynamics of the atom–photon scattering process (i.e. the absorption and then re-emission of the photon by the atom) compared with the timescales involved in the experiment, the photon–atom resonance scattering is described as a sudden change of the atom wavefunction accompanying the momentum transfer between the photon and the atom. Hence, we assume that each atom can be individually described by a pure state, and only when a collection of atoms is considered statistically does the decoherence effect arising from the photon-induced momentum displacements become apparent. More specifically, we use here the probability distribution of transverse momentum transfer to an atom in resonance fluorescence derived by Mandel [15, 16] from the angular distribution of spontaneously emitted photons.

According to such a model, we present here a functional dependence between the experimental observables, namely the fringe visibility and the phase shift, and the statistical distribution of photon–atom transversally transferred momentum. From this relationship, a direct connection is established between the coherence losses and subsequent revivals undergone by the atoms, which arise as a consequence of the statistical distribution of the sudden momentum shifts induced in the atomic wavefunction by the photons

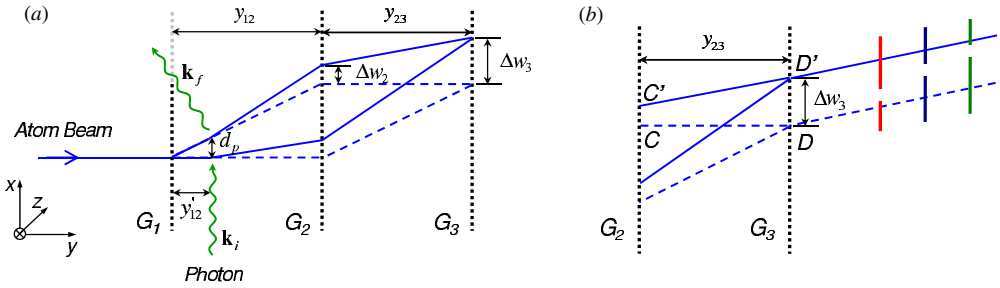


**Figure 1.** (*a*) Scheme of the experimental setup used by Chapman *et al* [5] to conduct their experiments on atom interferometry. Essentially, it consists of a Mach–Zehnder three-grating interferometer, where atoms are acted by external photons between the first and second gratings ($G_1$ and $G_2$). (*b*) Scheme showing the post-selection slits behind the third grating $G_3$; each one gives rise to a different post-selection momentum transfer distribution (see section 3).

(scattering-mediated momentum transfer processes). Furthermore, when some particular choices of momentum transfers are considered by selecting the outgoing atoms according to some prescribed momentum distributions, i.e. by post-selecting the atoms, a regain of the coherence is observed. As is shown, these results are in good agreement (both qualitatively and also quantitatively) when compared with the experimental data reported by Chapman *et al* [5]. Note therefore that this simple model thus provides a self-consistent explanation of the experiment based on first-principle-like arguments rather than only a best fitting to some suitable function.

This work is organized as follows. In section 2, to be self-contained, we start by briefly introducing the experimental setup used by Chapman *et al* [5] as well as a brief description of the two types of experiments they carried out. In section 3, we introduce our theoretical description of this experiment together with the analytical tools that arise from it, and later evaluate the fringe visibility and phase shift, which are compared with the experimental data. As will be seen, this entails the two features of a quantum particle within the same experiment: wave and corpuscle. In other words, with each individual atom that enters into and passes through the three-grating Mach–Zehnder interferometer, and then arrives at the detector, there is a wave associated, which is described by a coherent wavefunction or pure state. In section 4, results for different functional forms of the transversal momentum transfer distribution are analyzed and discussed. As is shown, when these results are directly compared with the experimental data reported in [5], a good agreement is found even without using any best-fit method, but just introducing the experimental parameters into the functional forms derived from our theoretical model. Finally, the main conclusions arising from this work are summarized in section 5.

## 2. Description of the experiment

In the experimental setup utilized by Chapman *et al* [5] (a sketch is shown in figure 1(*a*)), a beam of atomic sodium with a narrow velocity distribution is produced, collimated and launched through an atomic Mach–Zehnder interferometer. The interferometer consists of three 200 nm period nanofabricated Ronchi diffraction gratings (indicated by the vertical dotted lines in figure 1(*a*)) separated by $L = 65$ cm. Each grating acts as a coherent beam splitter [17], with the zeroth- and first-order maxima being the relevant ones.

A polarized laser beam behind the first grating, $G_1$, is switched on with the direction of the beam being parallel to this slit. This laser leads the atoms to a resonant excited state, from

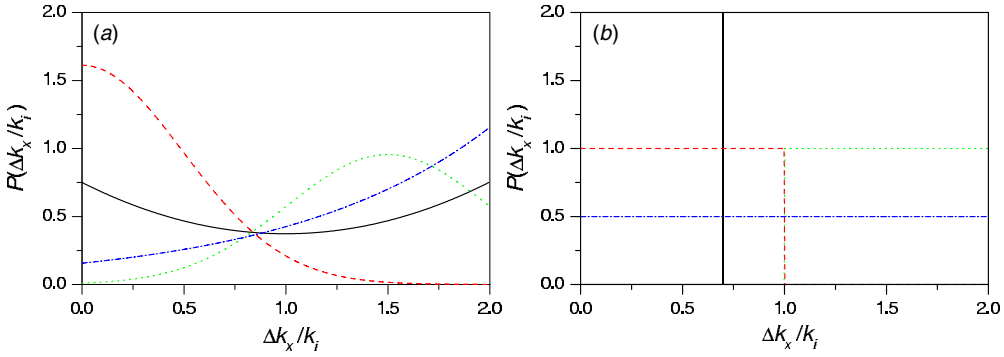


**Figure 2.** Transversal momentum transfer distributions as a function of the ratio between the transferred momentum and the incident photon wave number, $\Delta k_x/k_i$. In panel (*a*): bare momentum transfer distribution $P_0$ (black solid line) and post-selection momentum transfer distributions $P_{\rm I}$ (red dashed line), $P_{\rm II}$ (green dotted line) and $P_{\rm III}$ (blue dash–dotted line), as considered in the experiment [5] (the colors follow those of figure 1(*b*)). In panel (*b*): theoretical momentum transfer distributions $P_\delta$ (with $k_\delta = 0.7k_i$; vertical black solid line), $P_1$ (red dashed line), $P_2$ (green dotted line) and $P_c$ (blue dash–dotted line). All curves are normalized to unity within the interval $0 \leqslant \Delta k_x/k_i \leqslant 2$. See the text for particular details on the values of the parameter.

which they decay back to the ground state via spontaneous emission. The atomic flux collected behind the third grating, $G_3$ (see figure 1(*a*)), was then measured as a function of a shift $\Delta x_3$ produced in this grating along the $x$-axis, with the laser both off and on. This measurement was performed considering different values of the distance $y'_{12}$ between $G_1$ and the laser beam. Then, next, the same set of measurements was repeated, but adding a selection slit behind $G_3$, in front of the detector (see figure 1(*b*)). Each selection slit was associated with a particular range of values of the transferred transverse momentum.

The dependence of the measured values of the number of detected atoms on the shift $\Delta x_3$, given by

$$N(\Delta x_3) = \bar{N}\left[1 + C\cos\left(\frac{2\pi}{d_g}\,\Delta x_3 + \varphi\right)\right], \tag{1}$$

revealed interference [5]. In this expression, $\bar{N}$ is the average atom count rate, $d_g$ is the period of the grating and $C$ is the relative contrast (or fringe visibility). When the laser was off, the contrast $C$ was typically about 20% and the phase $\varphi$ was zero. When the laser was turned on, photon scattering events before and immediately after $G_1$ did not affect either the contrast $C$ or the phase. However, as $y'_{12}$ increases, the contrast decreases, first linearly and then it sharply falls to zero. Afterward, few revivals were observed. This behavior can be seen in figure 2 of [5], where the relative contrast (visibility) was represented as a function of $d_p/\lambda_i$, with $\lambda_i$ being the photon wavelength and

$$d_p = \left(\frac{2\pi}{kd_g}\right) y'_{12}. \tag{2}$$

Chapman *et al* [5] interpreted the quantity $d_p$ as 'the relative displacement of the two arms of the interferometer at the point of scattering'. However, Božić *et al* [14] pointed out that this quantity is equal to the separation between the two paths associated with the zeroth- and first-order interference maxima only in the far field, behind $G_1$. In contrast, in the near field, $d_p$ is equal to the distance between the prolongations of such paths. This distinction should be taken into account when interpreting the experimental data, since the photon–atom scattering

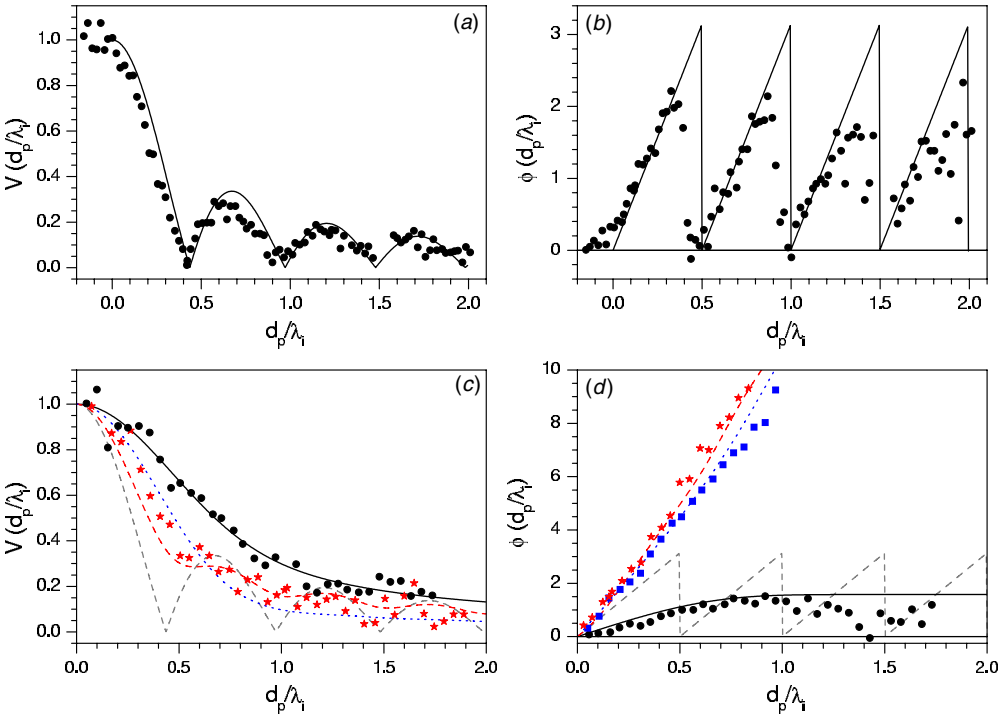


**Figure 3.** Functional dependence of the relative contrast (panels (*a*) and (*c*)) and the phase shift (panels (*b*) and (*d*)) on the momentum transfer distributions displayed in figure 2(*a*), and as a function of the ratio $d_p/\lambda_i$. Top: theoretical curves (solid line) and experimental data (black solid circles) for the bare momentum transfer distribution $P_0$. Bottom: theoretical curves (lines) and experimental data (symbols) for the post-selection momentum transfer distributions: $P_{\mathrm{I}}$ (black solid line/black solid circles), $P_{\mathrm{II}}$ (blue dotted line/blue squares; no experimental data were available for the corresponding relative contrast) and $P_{\mathrm{III}}$ (red dashed line/red stars). To compare with, the theoretical curves for the bare momentum transfer distribution $P_0$ have also been included, being denoted with the gray dashed line. The experimental data have been extracted from [5]; see the text for particular details on the values of the parameters.

events in this experiment take place in the near field. In this work this is explained in detail, taking into account the following fact:

$$y'_{12} = \frac{kd_g}{2\pi}\, d_p = \frac{d_p}{\lambda_i}\frac{kd_g}{k_i} = \frac{d_p}{\lambda_i}\frac{L_T}{2}\frac{\lambda_i}{d_g}, \tag{3}$$

where $L_T = 2d_g^2/\lambda$ is the so-called Talbot distance [18]. In the experiment, the ratio $d_p/\lambda_i$ ranges between 0 and 2. From the values of the other experimental parameters, it follows that $y'_{12} \in [0, 19.09]$ mm and the Talbot distance is $L_T = 6.48$ mm.

The same set of measurements was repeated, but this time adding a selection slit behind $G_3$, in front of the detector (see figure 1(*b*)). More specifically, this was done by arranging slits at three different positions, each selection slit being associated with a particular range of values of the transverse momentum $\Delta k_x$ transferred to the atom (i.e. with a particular momentum transfer distribution). This was possible because the deflection of the atom at the third grating, $\Delta w_3$, is proportional to $\Delta k_x$, the transverse momentum transferred to the atom. The curves shown in figure 3 of [5] show a substantial regain of contrast over the whole range of values for $d_p/\lambda_i$. In particular, a 60% of the contrast lost at $d_p \approx \lambda_i/2$ was regained.

From these results, Chapman *et al* [5] concluded that the decrease of contrast to zero in the range $0 < d_p/\lambda_i < 0.5$ confirms the complementarity in quantum mechanics, which suggests that the fringe contrast must disappear when it is possible to acquire which-way information, i.e. for $d_p/\lambda_i > 0.5$. Consequently, one should expect that beyond this value no coherence should be possible. In contrast, the experiment revealed that the atomic coherence displayed revivals in the relative contrast beyond the first zero, thus allowing the atoms to also display some wave-like behavior beyond the limits of complementarity. Furthermore, in the second part of the experiment, it was also observed that the coherence could be regained; actually, no zero values were observed in the relative contrast.

In our opinion, analyzing these kinds of experiments in terms of the idea of complementarity might be confusing, though it is very widespread. This was already pointed out by Englert [19] in 1996, who warned about the misunderstandings that may arise from the use of concepts like wave-particle duality unless they are clearly specified and disambiguated. As is shown below, in the model described here, such concepts, namely wave and particle, are not mutually exclusive, but they both coexist in the experiment, giving a good account of the experimental data. In particular, the wave aspect of the atom is kept all the way through the interferometer, the photon only causing a deviation of its translational motion (due to the kick and subsequent momentum transfer during the scattering event).

Having in mind these ideas and the scheme displayed in figure 1(*a*), in the derivations presented below, we assume that the atomic beam incident onto the grating $G_1$ (at $y = 0$) can be well approximated by a monochromatic or plane wave of finite transverse width with wavelength $\lambda$ and wave vector $\mathbf{k} = (2\pi/\lambda)\hat{\mathbf{y}}$. If the atomic beam cross-section is also assumed to be wide enough (in the experiment, this cross-section is about two orders of magnitude larger than the grating period [20]), not only it will cover a relatively large number of slits, but also an important extension along the $z$-direction. This causes a symmetry along the $z$-direction, which allows us to simplify the analysis by reducing it to the $XY$-plane (for fixed $z$, e.g., $z = 0$).

## 3. Theoretical approach

### *3.1. Atom's wavefunction evolution accompanying atom's passage through the interferometer*

Taking into account the description of the experiment made above, now we are going to analyze it here according to our model. Thus, consider the incident atomic wavefunction associated with atoms having a velocity $v$ is given by

$$\Psi_{\mathrm{inc}}(x, y, t) = \mathrm{e}^{-\mathrm{i}\omega t}\,\mathrm{e}^{\mathrm{i}ky}\psi_{\mathrm{inc}}(x), \tag{4}$$

where $\hbar\omega = \hbar^2k^2/2m$, $v = \hbar k/m$ and $\psi_{\mathrm{inc}}(x)$ describes the width of the initial wavefunction along the transverse direction. In the paraxial approximation, the outgoing wave evolving freely after the diffraction caused by $G_1$ is approximated by

$$\Psi(x, y, t) = \mathrm{e}^{-\mathrm{i}\omega t}\,\mathrm{e}^{\mathrm{i}ky}\psi^{\mathrm{tr}}(x, t). \tag{5}$$

This function is a product of the plane wave along the longitudinal $y$-direction by the 'transverse' wavefunction

$$\psi^{\mathrm{tr}}(x, t) = \frac{1}{\sqrt{2\pi}}\int_{-\infty}^{\infty} c(k_x)\,\mathrm{e}^{\mathrm{i}k_x x - i\hbar k_x^2 t/2m}\,\mathrm{d}k_x = \frac{1}{\sqrt{2\pi}}\int_{-\infty}^{\infty} C(k_x, t)\,\mathrm{e}^{\mathrm{i}k_x x}\,\mathrm{d}k_x \tag{6}$$

which describes the evolution along the $x$-direction. The function $c(k_x)$ is the Fourier transform of the function $\psi^{\mathrm{tr}}(x, 0)$ which is determined by $\psi_{\mathrm{inc}}(x)$ through the relation

$$\psi^{\mathrm{tr}}(x, 0) = T(x)\psi_{\mathrm{inc}}(x), \tag{7}$$

where $T(x)$ is the given transmission function of the grating $G_1$ located at $y = 0$. It is also the transmission function of grating $G_2$. More explicitly,

$$c(k_x) = \frac{1}{\sqrt{2\pi}} \int_{-\infty}^{\infty} T(x)\psi_{\text{inc}}(x)\, \mathrm{e}^{-\mathrm{i}k_x x}\, \mathrm{d}x, \tag{8}$$

$$C(k_x, t) = \frac{1}{\sqrt{2\pi}} \int_{-\infty}^{\infty} \psi^{\text{tr}}(x, t)\, \mathrm{e}^{-\mathrm{i}k_x x}\, \mathrm{d}x = c(k_x)\, \mathrm{e}^{\mathrm{i}k_x^2 \hbar t/2m}, \tag{9}$$

Evidently, $C(k_x, t)$ is the time-dependent transverse wavefunction in momentum representation.

Taking into account the length scales involved in the experiment, the paraxial approximation can be considered a good approximation. This implies, first, that the particle motion parallel to the $y$-direction can be treated as a quasi-classical (uniform) motion, i.e. satisfying the relation $y = vt$, with $v = \hbar k/m = 2\pi\hbar/\lambda$. Second, the wavefunction (7) behind the grating $G_1$ is such that $c(k_x)$ is relevant only for $k_x^2 \ll k_y^2 \approx k^2 = k_x^2 + k_y^2$ (in other words, the spreading of the wavefunction is much slower than its propagation along the $y$-direction [21]). Accordingly, equation (6) can be parameterized in terms of the $y$-coordinate or, equivalently, the (propagation) time $t$.

In the passage from $G_2$ to $G_3$ as well as beyond $G_3$, a similar analysis can be conducted (see below). However, at a time $t'_{12}$ and a distance $y'_{12} = vt'_{12} = (\hbar k/m)t'_{12}$ after the grating $G_1$, the atom absorbs and re-emits a photon. This process induces a sudden change $\Delta k_x$ in the atomic transverse momentum which is accompanied by the sudden change of the evolution of the atom's wavefunction. Arsenović *et al* [13] determined the evolution of the atom's wavefunction after photon–atom scattering by assuming that the atom's wavefunction in momentum representation after photon–atom scattering $C_{\Delta k_x}(k_x, t)$ has to satisfy

$$|C_{\Delta k_x}(k_x, t'_{12})|^2 = |C(k_x - \Delta k_x, t'_{12})|^2. \tag{10}$$

The corresponding transverse wavefunction at time $t'_{12}$ in accordance with (6) is then given by

$$\psi^{\text{tr}}_{\Delta k_x}(x, t'_{12}) = \frac{1}{\sqrt{2\pi}} \int_{-\infty}^{\infty} C_{\Delta k_x}(k_x, t'_{12})\, \mathrm{e}^{\mathrm{i}k_x x}\, \mathrm{d}k_x. \tag{11}$$

It should satisfy

$$\left|\psi^{\text{tr}}_{\Delta k_x}(x, t'_{12})\right|^2 = \left|\psi^{\text{tr}}(x, t'_{12})\right|^2. \tag{12}$$

As shown by Arsenović *et al* [13], from equations (9)–(11) it follows that condition (12) will be fulfilled if

$$C_{\Delta k_x}(k_x, t'_{12}) = C(k_x - \Delta k_x, t'_{12}). \tag{13}$$

Substituting (13) into (11) and then using (9), one finds that just after the photon–atom scattering event, the atomic wavefunction becomes

$$\psi^{\text{tr}}_{\Delta k_x}(x, t'_{12}) = \frac{1}{\sqrt{2\pi}}\, \mathrm{e}^{-\mathrm{i}\Delta k_x^2 \hbar t'_{12}/2m} \int_{-\infty}^{\infty} c(k_x - \Delta k_x)\, \mathrm{e}^{-\mathrm{i}k_x^2 \hbar t'_{12}/2m + \mathrm{i}k_x(x + \Delta x_0)}\, \mathrm{d}k_x, \tag{14}$$

where

$$\Delta x_0 = \frac{\Delta k_x \hbar t'_{12}}{m} = \left(\frac{\Delta k_x}{k}\right) y'_{12}. \tag{15}$$

Assuming that (14) keeps the same form at any $t > t'_{12}$, we may write

$$\psi^{\text{tr}}_{\Delta k_x}(x, t) = \frac{1}{\sqrt{2\pi}}\, \mathrm{e}^{-\mathrm{i}\Delta k_x^2 \hbar t/2m} \int_{-\infty}^{\infty} c(k_x - \Delta k_x)\, \mathrm{e}^{-\mathrm{i}k_x^2 \hbar t/2m + \mathrm{i}k_x(x + \Delta x_0)}\, \mathrm{d}k_x. \tag{16}$$

By changing now the integration variable $k'_x = k_x - \Delta k_x$, (16) transforms into

$$\psi_{\Delta k_x}(x,t) = \mathrm{e}^{\mathrm{i}\Delta k_x(x+\Delta x_0)-i\Delta k_x^2\hbar t/m}\int_{-\infty}^{\infty} c(k'_x)\,\mathrm{e}^{-\mathrm{i}k'^2_x\hbar t/2m}\,\mathrm{e}^{\mathrm{i}k'_x(x+\Delta x_0-\hbar t\Delta k_x/m)}\,\mathrm{d}k'_x. \tag{17}$$

This wavefunction describes the evolution of (6) after the scattering event (i.e. for $t > t'_{12}$ or, equivalently, $y > y'_{12} = (\hbar k/m)t'_{12}$). After the scattering event the atom wavefunction evolves freely until it reaches the second grating $G_2$. It is important to note that the wavefunction $\psi_0^{\mathrm{tr}}(x,t)$, associated with $\Delta k_x = 0$, also describes the evolution of the wave behind the first grating when laser is off.

It is useful to parameterize wavefunction (17) in terms of coordinate $y$ using the relation $\hbar t/m = y/k$,

$$\psi_{\Delta k_x}(x, t = my/\hbar k) = \frac{1}{\sqrt{2\pi}}\,\mathrm{e}^{\mathrm{i}\Delta k_x(x+\Delta x_0)-\mathrm{i}\Delta k_x^2 y/k}\int_{-\infty}^{\infty} c(k'_x)\,\mathrm{e}^{-\mathrm{i}k'^2_x y/2k}\,\mathrm{e}^{\mathrm{i}k'_x(x+\Delta x_0-\Delta k_x y/k)}\,\mathrm{d}k'_x. \tag{18}$$

The integrals in (17) and (18) have no general analytic solution, except for large $t$ or $y$ values. In such a limit, when the dimensions of the diffracting object and the wavelength of the diffracted beam are relatively small compared with the typical propagation distances, the far-field or Fraunhofer condition, $kx'^2/y \ll 1$ (with $x'$ being a measure of the dimensions of the diffracting object), holds [22] and (18) can be approximated (see appendix A) by

$$\psi_0^{\mathrm{tr}}(x, t = my/\hbar k) = \sqrt{\frac{k}{2\mathrm{i}\pi y}}\,\mathrm{e}^{\mathrm{i}kx^2/2y}c(kx/y) \tag{19}$$

when the laser is off, and

$$\psi_{\Delta k_x}^{\mathrm{tr}}(x, t = my/\hbar k) = \sqrt{\frac{k}{2i\pi y}}\,\mathrm{e}^{\mathrm{i}k(x+\Delta x_0)^2/2y-i\Delta k_x^2 y/2k}c[k(x+\Delta x_0)/y - \Delta k_x] \tag{20}$$

for $\Delta k_x \in [0, 2k_i]$ and the laser on. By comparing (19) and (20), we conclude that the overall form of the atom probability density $|\psi_{\Delta k_x}^{\mathrm{tr}}(x,t)|^2$ is the same as for $|\psi_0^{\mathrm{tr}}(x,t)|^2$. However, the former will display a shift or displacement along the $x$-direction with respect to the latter given by

$$\Delta w_2 = \frac{\Delta k_x}{k}\,(y - y'_{12}) = \left(\frac{\Delta k_x}{k}\right)y - \Delta x_0. \tag{21}$$

The evolution of the wavefunction between $G_2$ and $G_3$ follows a similar description to the one prior to the scattering event. Thus, if the wavefunction incident onto $G_2$ is denoted as $\psi^{(2)}_{\mathrm{inc},\Delta k_x}(x) \equiv \psi^{\mathrm{tr}}_{\Delta k_x}(x, t = my_{12}^{-0}/\hbar k)$, which arises from evaluating (20) at $y = y_{12}^{-0}$, just before the second grating, then wavefunction evolution behind the second grating ($y > y_{12}$) is given by

$$\begin{aligned}\psi^{(2)}_{\Delta k_x}(x,t) &= \frac{1}{\sqrt{2\pi}}\int_{-\infty}^{\infty} c^{(2)}_{\Delta k_x}(k_x)\,\mathrm{e}^{\mathrm{i}k_x x-\mathrm{i}\hbar k_x^2 t/2m}\,\mathrm{d}k_x \\ &= \frac{1}{\sqrt{2\pi}}\int_{-\infty}^{\infty} C^{(2)}_{\Delta k_x}(k_x,t)\,\mathrm{e}^{\mathrm{i}k_x x}\,\mathrm{d}k_x,\end{aligned} \tag{22}$$

where the relation between the time $t$ and $y$ is now $y - y_{12} = vt$ and the momentum probability density reads as

$$c^{(2)}_{\Delta k_x}(k_x) = \frac{1}{\sqrt{2\pi}}\int_{-\infty}^{\infty} T(x)\psi^{(2)}_{\mathrm{inc},\Delta k_x}(x)\,\mathrm{e}^{-\mathrm{i}k_x x}\,\mathrm{d}x. \tag{23}$$

From (22) and (23), one finds by numerical integration that the probability density incident onto $G_3$ for a given value of $\Delta k_x \in [0, 2k_i]$ oscillates with period $d_g$. This oscillatory pattern

(figure 3 in [13]) is of finite width and its position along the $x$-axis depends on $\Delta k_x$. In other words, the oscillatory pattern corresponding to $\Delta k_x \neq 0$ is shifted with respect to the oscillatory pattern when the laser is off, by the quantity

$$\Delta w_3 = \frac{\Delta k_x}{k}\,(2y_{12} - y'_{12}) = \left(\frac{\Delta k_x}{k}\right) 2y_{12} - \Delta x_0, \tag{24}$$

which arises after considering the shift of the wavefunction at $G_2$ (according to (21)) and the influence of $\Delta k_x$ on the propagation direction of the wavefunction emerging from $G_2$. This estimate of $\Delta w_3$ is consistent with the shifts determined through the numerical evaluation of the squared modulus of $\psi^{(2)}_{\Delta k_z}(x, t = my_{23}/\hbar k)$ [13, 14].

### *3.2. Atomic flux behind the interferometer*

In order to compare the results obtained from the theoretical model exposed above with the experimental data [5], we first consider the number of atoms transmitted through $G_3$ that undergo a change of momentum $\Delta k_x$ during the scattering process. This number is proportional to

$$\tilde{T}(y'_{12}, \Delta k_x, \Delta x_3) = \int_{\text{slits}} \left|\psi^{(2)}_{\Delta k_x}(x, t = my_{23}/\hbar k)\right|^2 \mathrm{d}x, \tag{25}$$

where $\Delta x_3$ is a lateral shift of the third grating with respect to the alignment of $G_2$ and the integration limits extend over the region covered by the central maximum at $G_3$. By numerical integration with the wavefunction determined as described in the previous section, it has been found [13, 14] that the transmitted flux (25) is a simple periodic function:

$$\tilde{T}(y'_{12}, \Delta k_x, \Delta x_3) = a + b\cos(2\pi\,\Delta x_3/d_g + \Delta k_x d_p), \tag{26}$$

where $d_p$ is defined in (2), and $a$ and $b$ are constants independent of $y'_{12}$ and $\Delta k_x$. Far from the grating (i.e. large values of $y'_{12}$), the distance $d_p$ is equal to the separation between the paths associated with the zeroth- and first-order interference maxima of the atomic wave diffracted by $G_1$ (see figure 1(*a*)). However, near the grating the emergent diffraction pattern is far more complex than a series of well-defined paths, obeying a Talbot-like carpet structure [18]. This implies, as explained after (3) and in [13], that $d_p$ should not be interpreted as the distance between two atomic paths in the region covered by the laser light, for in this region there are, actually, many more paths than simply two, as is generally assumed [2, 5].

The results reported in [5] essentially come from two types of measurements. The first type consists of simply counting *all* atoms that pass through $G_3$; in the second type, only a certain *subset* of the transmitted atoms are counted or *post-selected*, in particular those with a certain momentum direction, which is done by positioning an additional slit beyond $G_3$ (see figure 1(*b*)). Therefore, the observable is not $\tilde{T}(y'_{12}, \Delta k_x, \Delta x_3)$ in general, but its integral over a set of transferred momenta $\Delta k_x$,

$$\begin{aligned} T(y'_{12}, \Delta x_3) &= \int_0^{2k_i} \tilde{P}(\Delta k_x)\tilde{T}(y'_{12}, \Delta k_x, \Delta x_3)\,\mathrm{d}(\Delta k_x) \\ &= \int_0^{2k_i} \tilde{P}(\Delta k_x)[a + b\cos(2\pi\,\Delta x_3/d_g + \Delta k_x d_p)]\,\mathrm{d}(\Delta k_x), \end{aligned} \tag{27}$$

where the weight $\tilde{P}(\Delta k_x)$ denotes the *transversal momentum transfer distribution* of the detected atoms. More specifically, this quantity is the product of the atom momentum transfer distribution $P_0(\Delta k_x)$ and the distribution function $P_s(\Delta k_x)$ characterizing the way how the atoms are selected (*post-selected*) by their momentum beyond the interferometer. That is, we have $\tilde{P}(\Delta k_x) = P_0(\Delta k_x)P_s(\Delta k_x)$. In particular, when the post-selection process will

be included, we shall refer to the normalized $\tilde{P}$ function as the *post-selection momentum transfer distribution*. Thus, if $P(\Delta k_x) \equiv \tilde{P}(\Delta k_x)/\Gamma$, with $\Gamma \equiv \int_0^{2k_i} \tilde{P}(\Delta k_x)\,\mathrm{d}(\Delta k_x)$, is the corresponding normalized distribution, it is straightforward to verify that (27) reads as

$$T(y'_{12}, \Delta x_3) = a + b\mathcal{V}\cos(2\pi\,\Delta x_3/d_g + \varphi), \tag{28}$$

where the quantities $\mathcal{V}$ and $\varphi$ represent the *fringe visibility* or *relative contrast* and the *phase shift*, respectively, and are determined through the relations

$$\mathcal{V} \equiv \sqrt{I_r^2 + I_i^2}, \qquad \tan\varphi \equiv \frac{I_i}{I_r}, \tag{29}$$

with

$$\begin{aligned} I_r &\equiv \int_0^{2k_i} P(\Delta k_x)\cos(\Delta k_x d_p)\,\mathrm{d}(\Delta k_x), \\ I_i &\equiv \int_0^{2k_i} P(\Delta k_x)\sin(\Delta k_x d_p)\,\mathrm{d}(\Delta k_x). \end{aligned} \tag{30}$$

From a practical point of view, in order to evaluate $\mathcal{V}$ and $\varphi$, it is useful to introduce the complex integral

$$I \equiv \int_0^{2k_i} P(\Delta k_x)\,\mathrm{e}^{i\Delta k_x d_p}\,\mathrm{d}(\Delta k_x) = I_r + \mathrm{i}I_i, \tag{31}$$

so that

$$\mathcal{V} = \sqrt{I \cdot I^*}, \qquad \varphi = -\frac{\mathrm{i}}{2}\,\ln\left(\frac{I}{I^*}\right). \tag{32}$$

Taking this into account together with the standard definition of fringe contrast [16], from (28) we find

$$\mathcal{C} = \frac{T_{\max} - T_{\min}}{T_{\max} + T_{\min}} = \frac{|b|}{a}\,\mathcal{V}. \tag{33}$$

When the laser is off, $\Delta k_x = 0$ and hence $T(y'_{12}, \Delta x_3) = \tilde{T}(y'_{12}, 0, \Delta x_3) = a + b\cos(2\pi\,\Delta x_3/d_g)$ and $\mathcal{C}_0 = |b|/a$. The relative contrast then reads

$$\frac{\mathcal{C}}{\mathcal{C}_0} = \mathcal{V}, \tag{34}$$

which is a function of the ratio $d_p/\lambda_i$ ($\lambda_i$ is the scattering photon wavelength), as will be seen below.

## 4. Numerical results

In order to compare with the experiment, below we present some calculations, where we have considered the same parameter values used in the experiment [5]: $v = 1400\ \mathrm{ms}^{-1}$, $k = m_{\mathrm{Na}}v/\hbar = 5.090\,67 \times 10^{11}\ \mathrm{m}^{-1}$, $\lambda_i = 589\ \mathrm{nm}$ ($k_i = 1.066\,75 \times 10^7\ \mathrm{m}^{-1}$), $y_{12} = y_{23} = 0.65\ \mathrm{m}$, $d_g = 2 \times 10^{-7}\ \mathrm{m}$ and $\delta = 1 \times 10^{-7}\ \mathrm{m}$. To evaluate the wavefunction, we have considered a total number of illuminated slits $n = 24$ in $G_1$, which is an acceptable range compared with experimental atomic beam cross-sections (i.e. the coherence length of the atoms arriving in the grating) [20].

Apart from the Mandel distribution [15], which accounts for the bare transversal momentum transfer distribution, to compare with the experiment we have also considered the three post-selection momentum transfer distributions used in the experiment, denoted by $P_{\mathrm{I}}$, $P_{\mathrm{II}}$ and $P_{\mathrm{III}}$. These distributions correspond to the combined effect of the momentum transfer process (described by Mandel's distribution) and three different particular selections (post-selections of atomic momenta (each one given by a different $P_s$ distribution), which

are achieved by arranging a slit behind $G_3$ at three different positions (see figure 1(*b*)). The dependence of these four momentum transfer distributions as a function of the ratio between the transferred momentum and the incident photon wave number, $\Delta k_x/k_i$, is displayed in figure 2(*a*). Apart from these distributions, we have also considered several other theoretical forms for the momentum transfer distribution of the detected atoms, which are of interest to further analyze and better understand the dependence of coherence and visibility on the experimental distributions. In particular, a Dirac $\delta$-function distribution ($P_\delta$) and three constant distributions, $P_c$, $P_1$ and $P_2$, uniform over the intervals $[0, 2k_i]$, $[0, k_i]$ and $[k_i, 2k_i]$, respectively. These four distributions are displayed in figure 2(*b*).

A straightforward evaluation according to the method indicated at the end of section 3.2 leads us to the following expressions for the visibility and phase shift associated with these distributions.

(i) As shown by Mandel [15], for photons incident with a momentum $k_i$, the transversal momentum transfer distribution can be expressed as [15, 16]

$$P_0(\Delta k_x) = \left(\frac{3}{8k_i}\right)\left[1 + \left(1 - \frac{\Delta k_x}{k_i}\right)^2\right]. \tag{35}$$

In this case, the visibility and phase shift read

$$\mathcal{V}_0 = \frac{3}{2}\frac{1}{k_i d_p}\left[\left(1 - \frac{1}{k_i^2 d_p^2}\right)\sin(k_i d_p) + \frac{1}{k_i d_p}\cos(k_i d_p)\right], \tag{36}$$

$$\varphi_0 = k_i d_p = \frac{2\pi d_p}{\lambda_i}, \tag{37}$$

which are both functions of the ratio $d_p/\lambda_i$ (black solid lines in figures 3(*a*) and (*b*)). As can be seen, we find good agreement between these theoretical expressions and the experimental data (black solid circles) without taking into account any fitting procedure. Both the coherence losses and subsequent regains are thus accounted for without abandoning the idea of the pure state to describe the full evolution of the atom.

(ii) The case of $P_1$ is simulated by a half-Gaussian,

$$P_1(\Delta k_x) = 2/Nk_i\sqrt{\pi}\,\mathrm{e}^{-(\Delta k_x/Nk_i)^2}, \quad \Delta k_x \geqslant 0, \tag{38}$$

where $N$ determines the width of the Gaussian (here, we have chosen $N = 0.7$, so that $P_1(2k_i) \approx 0$). In this case (see appendix A),

$$\mathcal{V}_1 = \frac{|\mathrm{erf}(2/N - \mathrm{i}\alpha) + \mathrm{erf}(\mathrm{i}\alpha)|}{\mathrm{erf}(2/N)}\,\mathrm{e}^{-\alpha^2/4}, \tag{39}$$

$$\varphi_1 = \frac{1}{2\mathrm{i}}\,\ln\left[\frac{\mathrm{erf}(2/N - \mathrm{i}\alpha) + \mathrm{erf}(\mathrm{i}\alpha)}{\mathrm{erf}(2/N + \mathrm{i}\alpha) + \mathrm{erf}(-\mathrm{i}\alpha)}\right], \tag{40}$$

where $\alpha = Nk_i d_p$. As seen in figures 3(*c*) and (*d*) (black solid lines), there are no recurrences in $\mathcal{V}_1$ (they are completely damped), while $\varphi_1$ approaches a constant value of $\pi/2$ as $d_p/\lambda_i$ increases. Again, as can be seen, we find fair agreement with the experiment (black solid circles).

If instead of $\eta = 0$, one would choose $\eta = 1$, i.e. the mirror image of $P_1$ with respect to $\Delta k_x = k_i$, then

$$\mathcal{V}_1' = \frac{|\mathrm{erf}(2/N - \mathrm{i}\alpha) + \mathrm{erf}(\mathrm{i}\alpha)|}{\mathrm{erf}(2/N)}\,\mathrm{e}^{-\alpha^2/4}, \tag{41}$$

$$\varphi_1' = 2k_i d_p + \frac{1}{2i}\,\ln\left[\frac{\mathrm{erf}(2/N + \mathrm{i}\alpha) + \mathrm{erf}(-\mathrm{i}\alpha)}{\mathrm{erf}(2/N - \mathrm{i}\alpha) + \mathrm{erf}(\mathrm{i}\alpha)}\right]. \tag{42}$$

That is, the visibility is the same in both cases, but $\varphi_{\rm I}' = 2k_i d_p - \varphi_{\rm I}$ is an increasing linear function of $d_p/\lambda_i$ (after $\varphi_{\rm I}$ reaches its maximum, steady value).

(iii) For $P_{\rm II}$ we consider a displaced Gaussian,

$$P_{\rm II}(\Delta k_x) = 2/Nk_i\sqrt{\pi}[1 + \mathrm{erf}\ (1/2N)]\,\mathrm{e}^{-[(\Delta k_x - 3k_i/2)/Nk_i]^2}, \tag{43}$$

with its maximum at $\Delta k_x = 3k_i/2$ and $N = 0.7$, as before, so that $P_{\rm II}(2k_i + 3k_i/2) \approx 0$. With this, we find

$$\mathcal{V}_{\rm II} = \frac{|\mathrm{erf}(1/2N - \mathrm{i}\alpha) + \mathrm{erf}(3/2N + \mathrm{i}\alpha)|}{\mathrm{erf}(1/2N) + \mathrm{erf}(3/2N)}\,\mathrm{e}^{-\alpha^2/4}, \tag{44}$$

$$\varphi_{\rm II} = \frac{3k_i d_p}{2} + \frac{1}{2i}\,\ln\left[\frac{\mathrm{erf}\ (1/2N - \mathrm{i}\alpha) + \mathrm{erf}\ (3/2N + \mathrm{i}\alpha)}{\mathrm{erf}\ (1/2N + \mathrm{i}\alpha) + \mathrm{erf}\ (1/2N - \mathrm{i}\alpha)}\right], \tag{45}$$

which are represented by blue dotted lines in figures 3(*c*) and (*d*). In this case, since there relative contrast is very similar to that found for $P_{\rm I}$, no experimental data were reported. We only have experimental results for the phase shift (blue squares in figure 3(*d*)), where good agreement is also found.

(iv) $P_{\rm III}$ is described by means of an increasing exponential,

$$P_{\rm III}(\Delta k_x) = \epsilon/k_i(1 - \mathrm{e}^{-2\epsilon})\,\mathrm{e}^{\epsilon(\Delta k_x/k_i - 2)}, \tag{46}$$

where $\epsilon = 1$ is the increase rate (see blue dash–dotted line in figure 2(*a*)). This distribution leads to

$$\mathcal{V}_{\rm III} = \frac{\epsilon}{1 - \mathrm{e}^{-2\epsilon}}\,\frac{\sqrt{1 + \mathrm{e}^{-4\epsilon} - 2\mathrm{e}^{-2\epsilon}\cos(2k_i d_p)}}{\sqrt{\epsilon^2 + (k_i d_p)^2}}, \tag{47}$$

$$\varphi_{\rm III} = (\tan)^{-1}\left\{\frac{\sin(2k_i d_p - \phi) - \mathrm{e}^{-2\epsilon}\sin\phi}{\cos(2k_i d_p - \phi) - \mathrm{e}^{-2\epsilon}\cos\phi}\right\}, \tag{48}$$

where $\phi = (\tan)^{-1}(k_i d_p/\epsilon)$. As seen in figures 3(*c*) and (*d*) (red dashed lines), now $\mathcal{V}$ present some damped recurrences and there is a significant phase shift. The same trend is also observed in the experimental data (red stars), which follow very closely the behavior of the theoretically predicted curves.

There are several simple cases of particular interest, because *grosso modo* they capture the essential features of the distributions used in the experiment, which are the finite, uniform momentum transfer distributions within the interval $[k_1, k_2] \subset [0, 2k_i]$, being zero everywhere else,

$$P_u(\Delta k_x) = \frac{1}{k_2 - k_1}, \tag{49}$$

for $\Delta k_x \in [k_1, k_2]$. For this form, we find

$$\mathcal{V}_u = \left|\mathrm{sinc}\left[\frac{(k_2 - k_1)d_p}{2}\right]\right|, \tag{50}$$

$$\varphi_u = \frac{(k_2 + k_1)d_p}{2}. \tag{51}$$

As can be noted, the visibility is given in terms of the half-distance between the limits of the interval, $(k_2 - k_1)/2$, while the phase shift is proportional to their half-sum, $(k_2 + k_1)/2$, which corresponds to the average momentum. This implies that the visibility will decay and oscillate faster as both $k_1$ and $k_2$ approach the limits of the interval, the phase behaving in a similar manner (i.e. increasing). In contrast, if $k_1 \to k_2$, we will be approaching the limit described by $P_\delta$: $\mathcal{V}_u$ will oscillate more and more slowly (behaving almost constant up to very large values of $d_p/\lambda_i$), while its phase will approach $k_2 d_p$. Now we will analyze each of these cases separately.

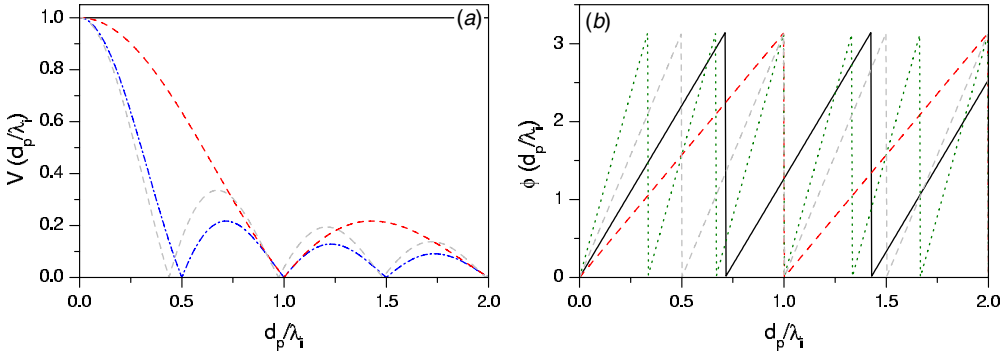


**Figure 4.** Functional dependence of the relative contrast (a) and the phase shift (b) on the momentum transfer distributions displayed in figure 2(*b*): $P_\delta$ (black solid line), $P_1$ (red dashed line), $P_2$ (green dotted line; $\mathcal{V}_2 = \mathcal{V}_1$ and no line can be seen) and $P_c$ (blue dash–dotted line). To compare with, the theoretical curves for the bare momentum transfer distribution $P_0$ have also been included, being denoted by the gray dashed line. See the text for particular details on the values of the parameter.

(a) For $P_\delta(\Delta k_x) = \delta(\Delta k_x - k_\delta)$ the visibility is constant and equal to unity along the interval $[0, 2k_i]$ (see black solid line in figure 4(*a*)). This means that a monochromatic event does not destroy the coherence of the atom wavefunction, but only produces a phase shift $\varphi_\delta = k_\delta d_p$ (see figure 3(*b*)).

(b) In the case $k_1 = 0$ and $k_2 = 2k_i$, $P_c(\Delta k_x) = 1/2k_i$, which is a rough approximation to $P_0$. Here, we find

$$\mathcal{V}_c = \frac{|\sin(k_i d_p)|}{k_i d_p}, \tag{52}$$

$$\varphi_c = k_i d_p. \tag{53}$$

(c) If $k_1 = 0$ and $k_2 = k_i$, we have $P_1(\Delta k_x) = 1/k_i$, which roughly describes $P_1$ and renders

$$\mathcal{V}_1 = \frac{|\sin(k_i d_p/2)|}{k_i d_p/2}, \tag{54}$$

$$\varphi_1 = \frac{k_i d_p}{2}. \tag{55}$$

(d) And, $k_1 = k_i$ and $k_2 = 2k_i$, we have $P_2(\Delta k_x) = 1/k_i$, which can be an approximation to either $P_1'$, $P_{\mathrm{II}}$ or $P_{\mathrm{III}}$, and gives rise to

$$\mathcal{V}_2 = \frac{|\sin(k_i d_p/2)|}{k_i d_p/2}, \tag{56}$$

$$\varphi_2 = \frac{3k_i d_p}{2}. \tag{57}$$

Note that in this case and in the previous one, the visibility is the same, but not the phase shifts, which increase three times faster for $P_2$ than for $P_1$.

As can be noted, the functional forms found with our model for the visibility and the phase shift associated with the different momentum transfer distributions are in good agreement with those reported in [5].

As can be noted, $\mathcal{V}_c$ vanishes for $d_p/\lambda_i = n/2$, with $n$ being an integer, while $\mathcal{V}_1$ and $\mathcal{V}_2$ vanish when $d_p/\lambda_i = n$. This is related to the fact that, for these three distributions, the integrand in (30) is a periodic function of $\Delta k_x$, with the period $2\pi/d_p$. For $P_c$ the integration in

(30) is carried out over the interval $[0, 2k_i]$, which contains an integer number of periods when $d_p/\lambda_i = n/2$. For $P_1$ and $P_2$ the integration is performed over the intervals $[0, k_i]$ and $[k_i, 2k_i]$, respectively, which contain an integer number of periods when $d_p/\lambda_i = n$. Nevertheless, it is worth going further and analyzing the physical reasons why the zeros of $\mathcal{V}_c$, $\mathcal{V}_1$ and $\mathcal{V}_2$ appear at these values of $d_p/\lambda_i$. To start with, let us remember that the phase $\Delta k_x d_p$ that appears in $\tilde{T}(y'_{12}, \Delta k_x, \Delta x_3)$ arises as a consequence of the shift $\Delta w_3$ along the $x$-axis at $G_3$ displayed by the atom wavefunction after the change of atomic transverse momentum due to photon–atom scattering. This shift, which is explicitly given by (24), contains the term $\Delta x_0$. The latter is of the order of the grating constant $d_g$, as can be noted if we define $\Delta k_x = \eta k_i$, with $0 \leqslant \eta \leqslant 2$ for $P_c$, $0 \leqslant \eta \leqslant 1$ for $P_1$ and $1 \leqslant \eta \leqslant 2$ for $P_2$. Thus, taking into account explicitly the value of $d_p$, we find $\Delta x_0 = (d_p/\lambda_i)\eta d_g$, which implies $0 \leqslant \Delta x_0 \leqslant (d_p/\lambda_i)2d_g$ for $P_c$, $0 \leqslant \Delta x_0 \leqslant (d_p/\lambda_i)d_g$ for $P_1$ and $(d_p/\lambda_i)d_g \leqslant \Delta x_0 \leqslant (d_p/\lambda_i)$ for $P_2$. Therefore, when $d_p/\lambda_i = 0.5$, $\Delta x_0$ lies within the intervals $[0, d_g]$, $[0, d_g/2]$ or $[d_g/2, d_g]$ depending on whether we have $P_c$, $P_1$ or $P_2$, respectively. This is why in the case of a uniform momentum transfer distribution along the interval $[0, 2k_i]$, the total number of detected atoms (27) does not depend on the lateral shift $\Delta x_0$ at $G_3$ and the contrast is zero. However, if the transferred momentum spans the interval $[0, k_i]$, the displacement of the wavefunction spans half the grating constant and, therefore, the number of detected atoms will depend on the lateral shift at $G_3$, then the contrast being greater than zero. On the other hand, when $d_p/\lambda_i = 1$, $\Delta x_0$ lies within the intervals $[0, 2d_g]$, $[0, d_g]$ and $[d_g, 2d_g]$ for $P_c$, $P_1$ and $P_2$, respectively. In these three cases the displacements thus span an integer number of grating periods. Therefore, in any of these cases, the total number of detected atoms will not depend on the lateral shift at $G_3$ and the contrast will vanish (see figures 4(*a*) and (*b*)).

It is insightful to analyze the experimental outcomes in light of the constant distributions. One could therefore state that the contrast regain found in the experiment, compared with the Mandel distribution, arises from the change of the momentum transfer distribution of the detected atoms, which is an objective effect. Furthermore, the loss and revival of coherence in the case of the Mandel distribution are also objective effects, which are related to the properties of the atomic wavefunction incident onto $G_3$.

## 5. Conclusions

In spite of the details involved in entanglement-based models aimed at describing complementarity in experiments like the one analyzed here, appealing to simpler models is also of interest in order to understand the underlying physics, even if they are not fully complete. In the case dealt with here, we have considered a description based on the recoil of the wavefunction describing the diffracted beam when a photon impinges on it within the interferometer. This model not only allows us to obtain a nice description of the evolution of the wavefunction throughout the matter-wave Mach–Zehnder interferometer, but also to explain the losses (e.g. the total loss at $d_p = 0.5\lambda_i$), subsequent revivals (for $d_p/\lambda_i > 0.5$) and regains (for all values of $d_p$ of experimental interest) undergone by the (atom) fringe contrast in a very simple manner. In particular, we have presented here how such effects arise when the outgoing atomic probability density is sampled by a certain momentum distribution, either Mandel's bare momentum transfer distribution or the corresponding post-selection ones. In other words, these three effects can be attributed to the smearing out of the interference pattern induced by the distribution of transverse momentum that the photon or the post-selection process cause on the atomic beam.

In order to obtain some extra information, other momentum transfer distributions of theoretical interest have also been considered. In this regard, it was shown that, if the atoms

passing through $G_3$ could be selected in such a way that only those with a chosen value of transferred momentum would be detected, then the contrast measured would be constant, i.e. independent of $d_p/\lambda_i$ (see figure 4(*a*) for $P_\delta$). In contrast, if the statistical momentum distribution is constant along the interval $[0, 2k_i]$, the interference contrast will be a simple periodic function of $d_p/\lambda_i$ (see figure 4(*a*) for $P_c$). These distributions allow us to understand the more complex situations that take place in real experiments, where the momentum transfer distribution is given by the Mandel distribution. In this case, in light of the results obtained from the theoretical momentum transfer distribution (in particular for $P_c$, which is roughly similar; see figures 2(*a*) and (*b*)), we find how the losses and regains with $d_p/\lambda_i$ are associated with the symmetry of this function with respect to $\Delta k_x = k_i$ (compare the gray curve for $P_0$ with the blue dash–dotted one for $P_c$ in figure 4(*a*)).

We would like to stress that the conclusions obtained here are also in agreement with those found from post-selection experiments [23, 24] in neutron interferometry [9, 23, 25]. In this case, interference and coherence phenomena can be completely hidden due to general averaging effects, but they can be recovered even behind the interferometer if a proper post-selection measurement procedure is used. This indicates that interference in phase space has to be considered [24] rather than the simple wavefunction overlap criterion described by the coherence function.

## Acknowledgments

MD, MB and DA acknowledge support from the Ministry of Science of Serbia under Projects OI171005, OI171028 and III45016. ASS acknowledges support from the Ministerio de Economía y Competitividad (Spain) under Projects FIS2010-22082 and FIS2011-29596-C02-01, as well as for a 'Ramón y Cajal' Research Fellowship.

## Appendix A.

The approximations (19) and (20) in the far field have been obtained through the following series of transformations [13, 26]. First, the wavefunction is expressed in terms of the initial wavefunction behind the grating, which is done by substituting (7) and (8) into (18),

$$\psi^{\mathrm{tr}}_{\Delta k_x}(x,y) = \frac{1}{\sqrt{2\pi}}\,\mathrm{e}^{\mathrm{i}\Delta k_x(x+\Delta x_0)-\mathrm{i}\Delta k_x^2 y/k} \times \int_{-\infty}^{\infty}\mathrm{d}k'_x\,\frac{1}{\sqrt{2\pi}}\int_{-\infty}^{\infty}\mathrm{d}x'\psi^{\mathrm{tr}}(x',0^+)\,\mathrm{e}^{-\mathrm{i}k'_x x'}\,\mathrm{e}^{-\mathrm{i}k'^2_x y/2k}\,\mathrm{e}^{\mathrm{i}k'_x(x+\Delta x_0-\Delta k_x y/k)}, \tag{A.1}$$

keeping in mind that the linear relation $t = my/\hbar k$ between $t$ and $y$ always holds. Next, the integration over $k'_x$ in (A.1) is carried out taking into account the integral [27]

$$\int_{-\infty}^{\infty}\mathrm{e}^{-ux^2-vx}\,\mathrm{d}x = \sqrt{\frac{\pi}{u}}\,\mathrm{e}^{v^2/4u}, \tag{A.2}$$

if $\mathrm{Re}(u) > 0$, $\mathrm{Re}(v) > 0$ or $\mathrm{Re}(u) = 0$, $\mathrm{Im}(u) \neq 0$ and $\mathrm{Re}(v) = 0$, $\mathrm{Im}(v) \neq 0$. In doing so, we obtain the result

$$\psi^{\mathrm{tr}}_{\Delta k_x}(x,y) = \frac{1}{2\pi}\,\mathrm{e}^{\mathrm{i}\Delta k_x(x+\Delta x_0)-\mathrm{i}\Delta k_x^2 y/k}\int_{-\infty}^{\infty}\mathrm{d}x'\psi(x',0^+)\sqrt{\frac{k}{\mathrm{i}y}}\,\sqrt{2\pi}\,\mathrm{e}^{\mathrm{i}[k(x-x'+\Delta x_0)-\Delta k_x y]^2/2ky}. \tag{A.3}$$

In the far-field approximation, the quadratic terms, $x'^2$, in the exponent under the integral can be neglected, which yields

$$\psi^{\mathrm{tr}}_{\Delta k_x}(x,y) = \frac{1}{\sqrt{2\pi}}\sqrt{\frac{k}{y}}\,\mathrm{e}^{-\mathrm{i}\pi/4+\mathrm{i}\Delta k_x(x+\Delta x_0)-\mathrm{i}\Delta k_x^2 y/k}\,\mathrm{e}^{\mathrm{i}[k(x+\Delta x_0)-\Delta k_x y]^2/2ky} \times \int_{-\infty}^{\infty}\mathrm{d}x'\psi(x',0^+)\,\mathrm{e}^{\mathrm{i}[k(x+\Delta x_0)-\Delta k_x y]x'/y}. \tag{A.4}$$

After recognizing in the latter equation the expression from (8), we find the form (20) of the wavefunction valid in the far field,

$$\psi^{\mathrm{tr}}_{\Delta k_x}(x,y) = \sqrt{\frac{k}{\mathrm{i}y}}\,\mathrm{e}^{\mathrm{i}k(x+\Delta x_0)^2/2y-\mathrm{i}\Delta k_x^2 y/2k}c[k(x+\Delta x_0)/y-\Delta k_x]. \tag{A.5}$$

## Appendix B.

The analysis of Gaussian-shaped distributions (e.g. $P_{\mathrm{I}}$ and $P_{\mathrm{II}}$) can be tackled in a general fashion as follows. Consider the distribution is centered at $k_g = \eta k_i$, such that $0 \leqslant \eta \leqslant 2$, i.e.

$$P_g(\Delta k_x) = \gamma_g\,\mathrm{e}^{-[(\Delta k_x - k_g)/Nk_i]^2}. \tag{B.1}$$

Here, $N$ is some constant determining the width of the distribution and $\gamma_g$ is the normalizing prefactor,

$$\gamma_g = \frac{2}{\sqrt{\pi}Nk_i}[\mathrm{erf}(\phi_+)+\mathrm{erf}(\phi_-)]^{-1}, \tag{B.2}$$

with $\mathrm{erf}(z)$ being the error function and

$$\phi_+ = \frac{2k_i - k_g}{Nk_i} = \frac{2-\eta}{N}, \qquad \phi_- = \frac{k_g}{Nk_i} = \frac{\eta}{N}. \tag{B.3}$$

Taking into account (B.1), the integral (31) can be expressed as

$$I_g = \left[\frac{\mathrm{erf}(u_+)+\mathrm{erf}(u_-)}{\mathrm{erf}(\phi_+)+\mathrm{erf}(\phi_-)}\right]\mathrm{e}^{-\alpha^2/4+\mathrm{i}\eta k_i d_p}, \tag{B.4}$$

where $\alpha = Nk_i d_p$. Note in the numerator of (B.4) that the error functions are complex, since their arguments,

$$\begin{aligned} u_+ &= \frac{2k_i - k_g}{Nk_i} - \frac{\mathrm{i}\alpha}{2} = \frac{2-\eta}{N} - \frac{\mathrm{i}\alpha}{2}, \\ u_- &= \frac{k_g}{Nk_i} + \frac{\mathrm{i}\alpha}{2} = \frac{\eta}{N} + \frac{\mathrm{i}\alpha}{2}, \end{aligned} \tag{B.5}$$

are also complex numbers. Therefore, they will satisfy the properties $\mathrm{erf}(-z) = -\mathrm{erf}(z)$ and $\overline{\mathrm{erf}(z)} = \mathrm{erf}(\bar{z})$. From (B.4), the visibility and phase shift induced by $P_g$ are

$$\mathcal{V}_g = \frac{|\mathrm{erf}\,(u_+)+\mathrm{erf}\,(u_-)|}{\mathrm{erf}\,(\phi_+)+\mathrm{erf}\,(\phi_-)}\,\mathrm{e}^{-\alpha^2/4}, \tag{B.6}$$

$$\varphi_g = \eta k_i d_p + \frac{1}{2\mathrm{i}}\ln\left[\frac{\mathrm{erf}\,(u_+)+\mathrm{erf}\,(u_-)}{\mathrm{erf}\,(\bar{u}_+)+\mathrm{erf}\,(\bar{u}_-)}\right]. \tag{B.7}$$

These two expressions can be evaluated for the half-Gaussian and displaced Gaussian distributions considered in section 3 by simply setting $\eta = 0$ or $\eta = 3/2$, respectively.

## References


[1] Rauch H and Werner S A 2000 *Neutron Interferometry* (Oxford: Clarendon)
[2] Cronin A D, Schmiedmayer J and Pritchard D E 2009 *Rev. Mod. Phys.* **81** 1051
[3] Bohr N 1949 Discussion with Einstein on epistemological problems in atomic physics *Albert Einstein: Philosopher-Scientist* ed P A Schilpp (Evanston, IL: The Library of Living Philosophers) pp 200–41
[4] de Broglie L 1963 *Etude Critiques des Bases de l'Interpretation Acruelle de la Mecanique Ondulatoire* (Paris: Gauthier-Villars) (Engl. transl. (Amsterdam: Elsevier))
[5] Chapman M S, Hammond T D, Lenef A, Schmiedmayer J, Rubenstein R A, Smith E and Pritchard D E 1995 *Phys. Rev. Lett.* **75** 3783
[6] Feynman R, Leighton F and Sands M 1965 *The Feynman Lectures on Physics* vol 3 (Reading, MA: Addison-Wesley) pp 5–7
[7] Schmiedmayer J, Chapman M S, Ekstrom C R, Hammond T D, Kokorowski D A, Lenef A, Rubenstein R A, Smith E T and Pritchard D E 1997 Optics and interferometry with atoms and molecules *Atom Interferometry* ed P R Berman (New York: Academic) pp 1–83
[8] Mandel L 1962 *J. Opt. Soc. Am.* **52** 1335
[9] Badurek G, Rauch H and Summhammer H 1983 *Phys. Rev. Lett.* **51** 1015
[10] Wiseman H and Harrison F 1995 *Nature* **377** 584
[11] Storey E P, Tan S M, Collett M J and Walls D F 1994 *Nature* **367** 626
[12] Stern A, Aharonov Y and Imry Y 1990 *Phys. Rev.* A **41** 3436
[13] Arsenović D, Božić M, Sanz A S and Davidović M 2009 *Phys. Scr.* **T135** 014025
[14] Božić M, Arsenović D, Sanz A S and Davidović M 2010 *Phys. Scr.* **T140** 014017
[15] Mandel L 1979 *J. Opt., Paris* **10** 51
[16] Mandel L and Wolf E 1995 *Optical Coherence and Quantum Optics* (Cambridge: Cambridge University Press)
[17] Božić M, Dimić D and Davidović M 2009 *Acta Phys. Pol.* **116** 479
[18] Sanz A S and Miret-Artés S 2007 *J. Chem. Phys.* **126** 234106
[19] Englert B-G 1996 *Phys. Rev. Lett.* **77** 2154
[20] Keith D W, Ekstrom C R, Turchette Q A and Pritchard D E 1991 *Phys. Rev. Lett.* **66** 2693
[21] Sanz A S and Miret-Artés S 2008 *J. Phys. A: Math. Theor.* **41** 435303
[22] Elmore W C and Heald M A 1985 *Physics of Waves* (New York: Dover)
[23] Jacobson D L, Werner S A and Rauch H 1994 *Phys. Rev.* A **49** 3196
[24] Schleich W, Walls D F and Wheeler J A 1988 *Phys. Rev.* A **38** 1177
[25] Rauch H and Summhammer J 1992 *Phys. Rev.* A **46** 7284
[26] Davidović M, Arsenović D, Božić M, Sanz A S and Miret-Artés S 2008 *Eur. Phys. J. Special Topics* **160** 95
[27] Davidović M, Božić M and Arsenović D 2006 *J. Russ. Laser Res.* **27** 220